# Equation of state for neutron stars in SU(3) flavor symmetry

Tsuyoshi Miyatsu* and Myung-Ki Cheoun†
*Department of Physics, Soongsil University, Seoul 156-743, Korea*

Koichi Saito‡
*Department of Physics, Faculty of Science and Technology, Tokyo University of Science (TUS), Noda 278-8510, Japan, and J-PARC Branch, KEK Theory Center, Institute of Particle and Nuclear Studies, KEK, Tokai 319-1106, Japan*
(Received 8 April 2013; revised manuscript received 7 June 2013; published 8 July 2013)

Using several relativistic mean-field models (such as GM1, GM3, NL3, TM1, FSUGold, and IU-FSU) as well as the quark-meson coupling model, we calculate the particle fractions, the equation of state, the maximum mass, and radius of a neutron star within relativistic Hartree approximation. We also discuss in detail the role of nonlinear potentials involved in the mean-field models. In determining the couplings of the isoscalar, vector mesons to the octet baryons, we examine the extension of SU(6) spin-flavor symmetry to SU(3) flavor symmetry. Furthermore, we consider the strange ($\sigma^*$ and $\phi$) mesons and study how they affect the equation of state. We find that the equation of state in SU(3) symmetry can sustain a neutron star with mass of $(1.8 \sim 2.1)M_\odot$, even if hyperons exist inside the core. It is noticeable that the strange vector ($\phi$) meson and the variation of baryon substructure in matter also play important roles in supporting a massive neutron star.

DOI: 10.1103/PhysRevC.88.015802 PACS number(s): 26.60.Kp, 97.60.Jd, 21.80.+a, 21.30.Fe

## I. INTRODUCTION

Neutron stars, which comprise hadrons and leptons as remnants of supernovae explosions, may be believed to be cosmological laboratories for dense nuclear matter. However, their detailed properties, for instance, the mass, radius, and particle fractions in the core of a neutron star, are not fully understood yet, since the pioneering paper by Baade and Zwicky [1] and the first discovery of a neutron star by Hewish and Okoye [2]. Because the observed mass and/or radius of a neutron star can provide strong constraints on the equation of state (EoS) of dense nuclear matter, many theoretical discussions have been focused on the EoS to understand the structure of dense matter.

The typical mass of neutron stars is known to be around $1.4\,M_\odot$ ($M_\odot$ is the solar mass) [3]. The most famous, precisely observed pulsar is the binary pulsar, B1913 + 16 (the Hulse-Taylor pulsar), with the mass of $1.4398 \pm 0.0002\,M_\odot$ [4,5]. However, a few neutron stars whose masses are much heavier than $1.4\,M_\odot$ have recently been observed. For example, Shapiro delay measurements have indicated that the binary millisecond pulsar, J1614-2230, has the mass of $1.97 \pm 0.04\,M_\odot$ [6]. Furthermore, a new massive pulsar, J0348 + 0432, has recently been reported and the mass is estimated to be $2.01 \pm 0.04\,M_\odot$ [7]. Then, such heavy neutron stars have attracted a lot of interest not only in astrophysics but also in nuclear physics, because of the possibility of exotic degrees of freedom, such as quarks, gluons, and/or some unusual condensations of boson-like matter, in the core.

Recent studies have used relativistic mean-field (RMF) models (or relativistic Hartree models), including hyperons ($Y$), to calculate the EoS for a neutron star. However, it is quite difficult to explain the heavy neutron stars by such EoSs with the meson-baryon coupling constants based on SU(6) (quark model) symmetry, because the degrees of freedom of hyperons make the EoS very soft, and thus, the possible maximum mass of a neutron star is considerably reduced [8,9].

In Refs. [10,11], the properties of a neutron star have been studied in detail within relativistic Hartree-Fock (RHF) approximation. In those calculations, we have considered not only the tensor couplings of vector mesons to the octet baryons and the form factors at interaction vertices but also the change of the quark substructure of baryons in dense matter. The RHF calculations have been performed in two ways: one with the coupling constants determined by SU(6) symmetry, the other with the coupling constants based on SU(3) (flavor) symmetry (see also Ref. [12]). Then, we have found that the baryon composition of the core matter in SU(3) symmetry is considerably different from that in SU(6) symmetry. In SU(6) symmetry, all octet baryons usually appear in the density region below $\sim$1.2 fm$^{-3}$, while in the SU(3) calculation, only the $\Xi^-$ hyperon is produced. Furthermore, the medium modification of the baryon structure hardens the EoS for the core. Taking all those effects into account, we have obtained the maximum mass of a neutron star, which is consistent with J1614-2230. Therefore, it is very important to consider the Fock contribution, the extension from SU(6) symmetry to SU(3) symmetry, and the effect of the baryon structure variation in nuclear matter.

It is interesting to construct the EoS based on SU(3) symmetry in RMF approximation and to see how the symmetry extension affects the EoS and how nonlinear (NL) potentials involved in RMF models work at very high densities, because the RMF calculation is practically much simpler than the RHF one, and many studies have, thus, proposed many useful RMF models. Furthermore, some of those models are accurately calibrated by various experimental data not only on infinite

*tmiyatsu@ssu.ac.kr
†cheoun@ssu.ac.kr
‡koichi.saito@rs.tus.ac.jp

 

nuclear matter but also on finite nuclei. In this paper, we extend several popular RMF models, such as the GM1, GM3, NL3, TM1, FSUGold, and IU-FSU models, and study the properties of nuclear matter and the mass-radius relations of neutron stars using the isoscalar, vector-meson couplings to the octet baryons in SU(3) symmetry. We then compare the results in SU(3) symmetry with those in the (usual) SU(6) calculations.

In addition, we propose RMF models, including the effect of baryon structure variation in a dense medium. In such models, we also use the coupling constants determined in SU(3) symmetry and compare the results with those calculated in SU(6) symmetry. To take the variation of the in-medium baryon structure into account, we use the quark-meson coupling (QMC) [13,14] and the chiral quark-meson coupling (CQMC) [15] models. It is well recognized that the constituent quark mass in a hadron is generated by the quark condensate, $\langle\bar{q}q\rangle$. The quark mass (or $\langle\bar{q}q\rangle$) in nuclear matter may then be reduced from the value in vacuum, because of the condensed scalar ($\sigma$) field depending on the nuclear density, namely the Lorentz-scalar, attractive interaction in nuclear matter. The decrease of the quark mass leads to the variation of baryon structure at the quark level. Such an effect is considered self-consistently in the QMC model.

The CQMC model is an extended version of the QMC model, in which the quark-quark hyperfine interaction caused by the one-gluon exchange is included. In addition, the pion-exchange interaction based on chiral symmetry is also considered. The hyperfine interaction plays an impotent role in the baryon spectra in matter [15,16]. The QMC and CQMC models have been successfully applied in studying the properties of hadrons in nuclear matter [17], finite nuclei [18–20], hypernuclei [21,22], and neutron stars [10,11,23]. (For a review, see Ref. [24].)

Using those models, we calculate the particle fractions, the meson fields, and the EoS inside the core. Furthermore, we estimate the maximum mass and radius of a neutron star by solving the Tolman-Oppenheimer-Volkoff (TOV) equation [25,26]. In the present calculations, we also study the role of the strange mesons ($\sigma^*$ and $\phi$) in the EoS. In SU(3) symmetry, we then find that the models, except for GM3, FSUGold, and IU-FSU, can explain the masses of J1614-2230 and/or J0348 + 0432. In the GM3, FSUGold, and IU-FSU models, although the maximum mass cannot reach $1.97 \pm 0.04\,M_\odot$, the calculated mass is not far from that value. Therefore, the extension from SU(6) to SU(3) symmetry is very vital for sustaining a heavy neutron star. In addition, the strange vector-meson ($\phi$) and the effect of baryon structure variation also help prevent the collapse of a neutron star.

In RMF models, various types of NL potentials with respect to the meson fields are usually involved, and they are very significant to reproduce the saturation condition for symmetric nuclear matter and the properties of finite nuclei. Among them, especially the $c_3\omega^4$ term hardens the EoS at high density and, thus, enhances a neutron-star mass. Furthermore, the NL isoscalar-isovector coupling, $\Lambda_{\omega\rho}\omega^2\rho^2$, which is involved only in the FSUGold and IU-FSU models, plays a unique role in the particle fractions in the core. If the $\sigma$-$\Sigma$ and $\sigma^*$-$\Sigma$ coupling constants are determined so as to fit the (repulsive) mean-field potential for the $\Sigma$ in nuclear matter, the $\Sigma$ hyperon usually tends to be excluded in the core of a neutron star. However, in the FSUGold and IU-FSU models, the $\Sigma^-$ as well as the $\Lambda$ and $\Xi^-$ can emerge with a considerable fraction even at rather low density, which may be caused by the $\Lambda_{\omega\rho}\omega^2\rho^2$ interaction. It is also important to investigate how such NL potentials behave in very dense matter.

This paper is organized as follows. In Sec. II, a brief review for RMF models based on quantum hadrodynamics (QHD) [27] is presented. The usual RMF models, the QMC and CQMC models, are then unified through the scalar polarizability. In Sec. III, the SU(3) extension in the coupling constants of the isoscalar, vector mesons is explained. The parameters in various models are determined in Sec. IV. Numerical results and discussions are addressed in Sec. V. Finally, we give a summary in Sec. VI.

## II. RELATIVISTIC MEAN-FIELD MODELS

For describing the properties of the core of a neutron star, we extend the usual Lagrangian density in RMF approximation to include not only the $\sigma$, $\omega$, and $\vec{\rho}$ mesons but also the strange mesons, namely the isoscalar, Lorentz scalar ($\sigma^*$), and vector ($\phi$) mesons. The $\sigma^*$ and $\phi$ mesons are predominantly composed of $\bar{s}s$ quarks. Because the charge neutrality and $\beta$ equilibrium conditions are imposed in the core, the leptons must be introduced as well. The Lagrangian density is, thus, chosen to be

$$\begin{aligned}\mathcal{L} = &\sum_B \bar{\psi}_B[i\gamma_\mu\partial^\mu - M_B^*(\sigma,\sigma^*) - g_{\omega B}\gamma_\mu\omega^\mu \\ &- g_{\phi B}\gamma_\mu\phi^\mu - g_{\rho B}\gamma_\mu\vec{\rho}^{\,\mu}\cdot\vec{I}_B]\psi_B \\ &+ \frac{1}{2}\left(\partial_\mu\sigma\partial^\mu\sigma - m_\sigma^2\sigma^2\right) + \frac{1}{2}\left(\partial_\mu\sigma^*\partial^\mu\sigma^* - m_{\sigma^*}^2\sigma^{*2}\right) \\ &+ \frac{1}{2}m_\omega^2\omega_\mu\omega^\mu - \frac{1}{4}W_{\mu\nu}W^{\mu\nu} + \frac{1}{2}m_\phi^2\phi_\mu\phi^\mu - \frac{1}{4}P_{\mu\nu}P^{\mu\nu} \\ &+ \frac{1}{2}m_\rho^2\vec{\rho}_\mu\cdot\vec{\rho}^{\,\mu} - \frac{1}{4}\vec{R}_{\mu\nu}\cdot\vec{R}^{\mu\nu} \\ &- U_{NL}(\sigma,\omega^\mu,\vec{\rho}^{\,\mu}) + \sum_\ell \bar{\psi}_\ell[i\gamma_\mu\partial^\mu - m_\ell]\psi_\ell, \end{aligned} \tag{1}$$

where

$$\begin{aligned} W_{\mu\nu} &= \partial_\mu\omega_\nu - \partial_\nu\omega_\mu, \quad P_{\mu\nu} = \partial_\mu\phi_\nu - \partial_\nu\phi_\mu, \\ \vec{R}_{\mu\nu} &= \partial_\mu\vec{\rho}_\nu - \partial_\nu\vec{\rho}_\mu, \end{aligned} \tag{2}$$

with $\psi_{B(\ell)}$ the baryon (lepton) field, $\vec{I}_B$ the isospin matrix for baryon $B$, and $m_\ell$ the lepton mass. The sum $B$ runs over the octet baryons, $N$ (proton and neutron), $\Lambda$, $\Sigma^{+,0,-}$, and $\Xi^{0,-}$, and the sum $\ell$ is for the leptons, $e^-$ and $\mu^-$. The $\omega$-, $\phi$-, and $\rho$-$B$ coupling constants are, respectively, denoted by $g_{\omega B}$, $g_{\phi B}$, and $g_{\rho B}$. In Eq. (1), $U_{\rm NL}$ is a NL potential, which is explained below.

When the baryons are treated as point-like objects (as in QHD), the effective baryon mass, $M_B^*$, in matter is simply expressed as

$$M_B^*(\sigma,\sigma^*) = M_B - g_{\sigma B}\sigma - g_{\sigma^* B}\sigma^*, \tag{3}$$

TABLE I. Values of $a_B$, $b_B$, $a'_B$, and $b'_B$ for the octet baryons in the QMC or CQMC model. We assume that the scalar, strange ($\sigma^*$) meson does not couple to the nucleon.

| $B$ | QMC | | | | CQMC | | | |
|---|---|---|---|---|---|---|---|---|
| | $a_B$ (fm) | $b_B$ | $a'_B$ (fm) | $b'_B$ | $a_B$ (fm) | $b_B$ | $a'_B$ (fm) | $b'_B$ |
| $N$ | 0.179 | 1.00 | – | – | 0.118 | 1.04 | – | – |
| $\Lambda$ | 0.172 | 1.00 | 0.220 | 1.00 | 0.122 | 1.09 | 0.290 | 1.00 |
| $\Sigma$ | 0.177 | 1.00 | 0.223 | 1.00 | 0.184 | 1.02 | 0.277 | 1.15 |
| $\Xi$ | 0.166 | 1.00 | 0.215 | 1.00 | 0.181 | 1.15 | 0.292 | 1.04 |

where $M_B$ is the mass in vacuum, and $g_{\sigma B}$ and $g_{\sigma^* B}$ are the $\sigma$- and $\sigma^*$-$B$ coupling constants, respectively. We hereafter call the model in which the baryons are structureless the QHD-type model.

In contrast, in the QMC and CQMC models, the coupling constants, $g_{\sigma B}$ and $g_{\sigma^* B}$, depend on the $\sigma$ and $\sigma^*$ fields, which reflects the variation of baryon structure in matter [14,24]. Such dependencies are caused by the attractive interactions due to the $\sigma$ and $\sigma^*$ exchanges. Thus, the in-medium baryon mass can be written as [23]

$$M_B^*(\sigma,\sigma^*) = M_B - g_{\sigma B}(\sigma)\sigma - g_{\sigma^* B}(\sigma^*)\sigma^*, \tag{4}$$

with the following, simple parametrizations [10,11,17,18,22]:

$$g_{\sigma B}(\sigma) = g_{\sigma B} b_B \left[1 - \frac{a_B}{2}(g_{\sigma N}\sigma)\right], \tag{5}$$

$$g_{\sigma^* B}(\sigma^*) = g_{\sigma^* B} b'_B \left[1 - \frac{a'_B}{2}(g_{\sigma^*\Lambda}\sigma^*)\right], \tag{6}$$

where $g_{\sigma N}$ and $g_{\sigma^*\Lambda}$ are, respectively, the $\sigma$-$N$ and $\sigma^*$-$\Lambda$ coupling constants at zero density. Here, we introduce four parameters, $a_B$, $b_B$, $a'_B$, and $b'_B$, for describing the mass, and their values are tabulated in Table I. The effect of the baryon structure variation at the quark level can be described with the parameters $a_B$ and $a'_B$. In addition, in the CQMC model, the extra parameters, $b_B$ and $b'_B$, are necessary to express the effect of hyperfine interaction between two quarks [15,16,22]. If we set $a_B = 0$ and $b_B = 1$, $g_{\sigma B}(\sigma)$ becomes identical to the $\sigma$-$B$ coupling constant in QHD. This is also true of the coupling $g_{\sigma^* B}(\sigma^*)$.

We here note that the RMF model with the coupling constants depending on the scalar mean-field value in matter (such as the QMC and CQMC models) seems similar to the density-dependent meson-exchange (DDME) model [28], where the coupling constants depend on the nuclear density and those are parametrized in terms of some specific functions. However, there are some remarkable differences between those models; for example, the couplings in the QMC and CQMC models are invariant under Lorentz transformation, while those in the DDME model may depend on the choice of a frame.

In the QHD-type model, we add the following NL potential to the Lagrangian density

$$U_{\rm NL}(\sigma,\omega^\mu,\vec{\rho}^{\,\mu}) = \tfrac{1}{3}g_2\sigma^3 + \tfrac{1}{4}g_3\sigma^4 - \tfrac{1}{4}c_3(\omega_\mu\omega^\mu)^2 - \Lambda_{\omega\rho}(\omega_\mu\omega^\mu)(\vec{\rho}_\mu\cdot\vec{\rho}^{\,\mu}), \tag{7}$$

so as to reproduce the measured properties of nuclear matter and finite nuclei, for example, the incompressibility of nuclear matter, $K_v$, the density dependence of symmetry energy, $a_4$, etc. Here, the potential involves four coupling constants, $g_2$, $g_3$, $c_3$, and $\Lambda_{\omega\rho}(\equiv \Lambda_v g_{\rho N}^2 g_{\omega N}^2)$.

In RMF approximation, the meson fields are replaced by the constant mean-field values: $\bar\sigma$, $\bar\omega$, $\bar\sigma^*$, $\bar\phi$, and $\bar\rho$ (the $\rho^0$ field). The equations of motion for the meson fields in uniform matter are, thus, given by

$$m_\sigma^2\bar\sigma + g_2\bar\sigma^2 + g_3\bar\sigma^3 = \sum_B g_{\sigma B} C_B(\bar\sigma)\rho_B^s, \tag{8}$$

$$m_{\sigma^*}^2\bar\sigma^* = \sum_B g_{\sigma^* B} C'_B(\bar\sigma^*)\rho_B^s, \tag{9}$$

$$\left(m_\omega^2 + 2\Lambda_{\omega\rho}\bar\rho^2\right)\bar\omega + c_3\bar\omega^3 = \sum_B g_{\omega B}\rho_B, \tag{10}$$

$$m_\phi^2\bar\phi = \sum_B g_{\phi B}\rho_B, \tag{11}$$

$$\left(m_\rho^2 + 2\Lambda_{\omega\rho}\bar\omega^2\right)\bar\rho = \sum_B g_{\rho B}(\vec{I}_B)_3\rho_B, \tag{12}$$

TABLE II. Coupling constants and properties of symmetric nuclear matter in the QMC and CQMC models. We assume that $g_{\sigma^* N} = 0$ and $g_{\sigma^*\Lambda} = g_{\sigma^*\Sigma}$. The hadron masses are taken as follows: $M_N = 939$ MeV, $M_\Lambda = 1116$ MeV, $M_\Sigma = 1193$ MeV, $M_\Xi = 1318$ MeV, $m_\sigma = 550$ MeV, $m_\omega = 783$ MeV, $m_\rho = 770$ MeV, $m_{\sigma^*} = 975$ MeV, and $m_\phi = 1020$ MeV. The saturation condition for symmetric nuclear matter is supposed to be $w_0 = -15.7$ MeV at $n_B^0 = 0.15$ fm$^{-3}$. The symmetry energy is taken to be $a_4 = 32.5$ MeV at $n_B^0$, and the slope parameter of the symmetry energy is denoted by $L$.[a]

| Vector symmetry | QMC | | CQMC | |
|---|---|---|---|---|
| | SU(6) | SU(3) | SU(6) | SU(3) |
| Coupling constants | | | | |
| $g_{\sigma N}$ | 8.28 | 8.28 | 8.50 | 8.50 |
| $g_{\omega N}$ | 8.24 | 7.98 | 9.45 | 9.14 |
| $g_{\rho N}$ | 4.38 | 4.38 | 4.29 | 4.29 |
| $g_{\phi N}$ | – | −2.72 | – | −3.12 |
| $g_{\sigma\Lambda}$ | 5.01 | 6.09 | 4.97 | 6.11 |
| $g_{\sigma\Sigma}$ | 2.45 | 3.53 | 3.24 | 4.51 |
| $g_{\sigma\Xi}$ | 2.67 | 4.83 | 2.59 | 4.84 |
| $g_{\sigma^*\Lambda}$ | 1.09 | 0.00[b] | 2.62 | 1.17 |
| $g_{\sigma^*\Xi}$ | 7.53 | 5.19 | 8.46 | 5.80 |
| Properties of symmetric nuclear matter | | | | |
| $M_N^*/M_N$ | 0.80 | 0.80 | 0.76 | 0.76 |
| $K_v$ (MeV) | 280 | 280 | 302 | 302 |
| $a_4$ (MeV) | 32.5 | 32.5 | 32.5 | 32.5 |
| $L$ (MeV) | 88.7 | 88.7 | 90.7 | 90.7 |

[a]The symmetry energy, $a_4$, is defined in terms of the 2nd derivative of the total energy with respect to the difference between proton and neutron densities, and the slope parameter, $L$, is then given by the derivative of $a_4$ with respect to the baryon density [41,42].

[b]Because the $\sigma$-meson contribution in the QMC model already gives $U_\Lambda^{(\Lambda)} = -8$ MeV at $n_B^0$, the additional, attractive force due to the $\sigma^*$ meson is not required.

TABLE III. Coupling constants and properties of symmetric nuclear matter in the GM1, GM3, and NL3 models. The relations, $g_{\sigma^*N} = 0$ and $g_{\sigma^*\Lambda} = g_{\sigma^*\Sigma}$, are assumed. For the NL3 model, we take $m_\sigma = 508.194$ MeV, $m_\omega = 782.501$ MeV, and $m_\rho = 763.000$ MeV [33]. The other masses are the same as in Table II.

| Vector symmetry | GM1 | | GM3 | | NL3 | |
|---|---|---|---|---|---|---|
| | SU(6) | SU(3) | SU(6) | SU(3) | SU(6) | SU(3) |
| | | | Coupling constants | | | |
| $g_{\sigma N}$ | 9.57 | 9.57 | 8.78 | 8.78 | 10.217 | 10.217 |
| $g_2$ (fm$^{-1}$) | 12.28 | 12.28 | 27.88 | 27.88 | 10.431 | 10.431 |
| $g_3$ | −8.98 | −8.98 | −14.40 | −14.40 | −28.885 | −28.885 |
| $g_{\omega N}$ | 10.61 | 10.26 | 8.71 | 8.43 | 12.868 | 12.450 |
| $g_{\rho N}$ | 4.10 | 4.10 | 4.27 | 4.27 | 4.474 | 4.474 |
| $g_{\phi N}$ | – | −3.50 | – | −2.88 | – | −4.250 |
| $g_{\sigma\Lambda}$ | 5.84 | 7.25 | 5.32 | 6.51 | 6.269 | 7.853 |
| $g_{\sigma\Sigma}$ | 3.87 | 5.28 | 2.85 | 4.04 | 4.709 | 6.293 |
| $g_{\sigma\Xi}$ | 3.06 | 5.87 | 2.83 | 5.20 | 3.242 | 6.408 |
| $g_{\sigma^*\Lambda}$ | 3.73 | 2.60 | 2.03 | 1.95 | 5.374 | 4.174 |
| $g_{\sigma^*\Xi}$ | 9.67 | 6.82 | 7.89 | 5.55 | 11.765 | 8.378 |
| | | | Properties of symmetric nuclear matter | | | |
| $n_B^0$ (fm$^{-3}$) | 0.153 | 0.153 | 0.153 | 0.153 | 0.148 | 0.148 |
| $w_0$ (MeV) | −16.3 | −16.3 | −16.3 | −16.3 | −16.299 | −16.299 |
| $M_N^*/M_N$ | 0.70 | 0.70 | 0.78 | 0.78 | 0.60 | 0.60 |
| $K_v$ (MeV) | 300 | 300 | 240 | 240 | 271.76 | 271.76 |
| $a_4$ (MeV) | 32.5 | 32.5 | 32.5 | 32.5 | 37.4 | 37.4 |
| $L$ (MeV) | 93.9 | 93.9 | 89.7 | 89.7 | 118.0 | 118.0 |

TABLE IV. Coupling constants and properties of symmetric nuclear matter in the TM1, FSUGold, and IU-FSU models. The relations, $g_{\sigma^*N} = 0$ and $g_{\sigma^*\Lambda} = g_{\sigma^*\Sigma}$, are assumed. For the TM1 model, we take $M_N = 938$ MeV and $m_\sigma = 511.198$ MeV [34], while, for the FSUGold and IU-FSU models, $m_\sigma = 491.500$ MeV, $m_\omega = 782.500$ MeV, and $m_\rho = 763.000$ MeV [35,36]. The other masses are the same as in Table II.

| Vector symmetry | TM1 | | FSUGold | | IU-FSU | |
|---|---|---|---|---|---|---|
| | SU(6) | SU(3) | SU(6) | SU(3) | SU(6) | SU(3) |
| | | | Coupling constants | | | |
| $g_{\sigma N}$ | 10.029 | 10.029 | 10.592 | 10.592 | 9.971 | 9.971 |
| $g_2$ (fm$^{-1}$) | 7.233 | 7.233 | 4.277 | 4.277 | 8.493 | 8.493 |
| $g_3$ | 0.618 | 0.618 | 49.856 | 49.856 | 0.488 | 0.488 |
| $c_3$ | 71.308 | 81.601 | 418.394 | 522.820 | 144.220 | 171.586 |
| $\Lambda_{\omega\rho}$[a] | – | – | 212.427 | 168.100 | 360.714 | 248.010 |
| $g_{\omega N}$ | 12.614 | 12.199 | 14.302 | 13.874 | 13.032 | 12.615 |
| $g_{\rho N}$ | 4.632 | 4.640 | 5.884 | 5.395 | 6.795 | 5.821 |
| $g_{\phi N}$ | – | −4.164 | – | −4.736 | – | −4.306 |
| $g_{\sigma\Lambda}$ | 6.170 | 7.733 | 6.501 | 8.295 | 6.090 | 7.680 |
| $g_{\sigma\Sigma}$ | 4.472 | 6.035 | 4.820 | 6.615 | 4.517 | 6.107 |
| $g_{\sigma\Xi}$ | 3.202 | 6.328 | 3.366 | 6.953 | 3.154 | 6.334 |
| $g_{\sigma^*\Lambda}$ | 5.015 | 3.691 | 5.994 | 4.458 | 5.476 | 4.204 |
| $g_{\sigma^*\Xi}$ | 11.516 | 8.100 | 13.071 | 9.147 | 11.915 | 8.437 |
| | | | Properties of symmetric nuclear matter | | | |
| $n_B^0$ (fm$^{-3}$) | 0.145 | 0.145 | 0.148 | 0.148 | 0.155 | 0.155 |
| $w_0$ (MeV) | −16.3 | −16.3 | −16.30 | −16.30 | −16.40 | −16.40 |
| $M_B^*/M_B$ | 0.634 | 0.634 | 0.61 | 0.61 | 0.61 | 0.61 |
| $K_v$ (MeV) | 281 | 284 | 230 | 252 | 231.2 | 237.7 |
| $a_4$ (MeV) | 36.9 | 36.9 | 32.59 | 32.59 | 31.30 | 31.30 |
| $L$ (MeV) | 110.9 | 110.8 | 60.3 | 66.6 | 47.2 | 54.6 |

[a]The coupling constant, $\Lambda_{\omega\rho}$, also varies, because it is defined by $\Lambda_{\omega\rho} = \Lambda_v g_{\rho N}^2 g_{\omega N}^2$, where $\Lambda_v$ takes the same value in both SU(3) and SU(6) cases.

where the scalar density, $\rho_B^s$, and the baryon density, $\rho_B$, read

$$\rho_B^s = \frac{1}{\pi^2}\int_0^{k_{F_B}} dk k^2 \frac{M_B^*(\bar\sigma,\bar\sigma^*)}{\left[k^2+M_B^{*2}(\bar\sigma,\bar\sigma^*)\right]^{1/2}}, \tag{13}$$

$$\rho_B = \frac{1}{\pi^2}\int_0^{k_{F_B}} dk k^2 = \frac{k_{F_B}^3}{3\pi^2}, \tag{14}$$

with $k_{F_B}$ being the Fermi momentum for baryon $B$.

In Eqs. (8) and (9), $C_B$ and $C'_B$ are, respectively, the scalar polarizabilities (or the scalar-density ratios) at the $\sigma$-$B$ and $\sigma^*$-$B$ interactions. Here, the scalar polarizabilities is defined by the ratio of the scalar density of a confined quark-field at finite density to that in vacuum. In the QMC or CQMC model, they can be expressed by the following parametrizations [10,11,21,23]:

$$C_B(\bar\sigma) = b_B[1-a_B(g_{\sigma N}\bar\sigma)], \tag{15}$$

$$C'_B(\bar\sigma^*) = b'_B[1-a'_B(g_{\sigma^*\Lambda}\bar\sigma^*)], \tag{16}$$

where the parameters $a_B$, $b_B$, $a'_B$, and $b'_B$ take the same values as in Eqs. (5) and (6) (see also Table I). In contrast, they become unity in the QHD-type model (recall $a_B = a'_B = 0$ and $b_B = b'_B = 1$).

The total energy density, $\epsilon$, and pressure, $P$, in the core then read

$$\begin{aligned}\epsilon = {}& \sum_B \frac{1}{\pi^2}\int_0^{k_{F_B}} dk k^2\left[k^2+M_B^{*2}(\bar\sigma,\bar\sigma^*)\right]^{1/2} \\ & + \frac{1}{2}m_\sigma^2\bar\sigma^2 + \frac{1}{3}g_2\bar\sigma^3 + \frac{1}{4}g_3\bar\sigma^4 + \frac{1}{2}m_{\sigma^*}^2\bar\sigma^{*2} \\ & + \frac{1}{2}m_\omega^2\bar\omega^2 + \frac{3}{4}c_3\bar\omega^4 + \frac{1}{2}m_\phi^2\bar\phi^2 + \frac{1}{2}m_\rho^2\bar\rho^2 + 3\Lambda_{\omega\rho}\bar\omega^2\bar\rho^2 \\ & + \sum_\ell \frac{1}{\pi^2}\int_0^{k_{F_\ell}} dk k^2\left[k^2+m_\ell^2\right]^{1/2},\end{aligned} \tag{17}$$

$$P = n_B^2\frac{\partial}{\partial n_B}\left(\frac{\epsilon}{n_B}\right), \tag{18}$$

where the total baryon density, $n_B$, is given by a sum of each baryon density

$$n_B = \sum_B \rho_B. \tag{19}$$

In the QHD-type model, the pressure can alternatively be expressed as

$$\begin{aligned}P = {}& \frac{1}{3}\sum_B \frac{1}{\pi^2}\int_0^{k_{F_B}} dk \frac{k^4}{\left[k^2+M_B^{*2}(\bar\sigma,\bar\sigma^*)\right]^{1/2}} - \frac{1}{2}m_\sigma^2\bar\sigma^2 \\ & - \frac{1}{3}g_2\bar\sigma^3 - \frac{1}{4}g_3\bar\sigma^4 - \frac{1}{2}m_{\sigma^*}^2\bar\sigma^{*2} + \frac{1}{2}m_\omega^2\bar\omega^2 + \frac{1}{4}c_3\bar\omega^4 \\ & + \frac{1}{2}m_\phi^2\bar\phi^2 + \frac{1}{2}m_\rho^2\bar\rho^2 + \Lambda_{\omega\rho}\bar\omega^2\bar\rho^2 \\ & + \frac{1}{3}\sum_\ell \frac{1}{\pi^2}\int_0^{k_{F_\ell}} dk \frac{k^4}{\left[k^2+m_\ell^2\right]}.\end{aligned} \tag{20}$$

## III. SU(3) SYMMETRY IN THE ISOSCALAR, VECTOR-MESON COUPLINGS

To study the EoS and the properties of neutron stars, it is very interesting to extend SU(6) spin-flavor symmetry based on the quark model to the more general SU(3) flavor symmetry [12,29]. Restricting our interest to three quark flavors (up, down, and strange), SU(3) symmetry can be regarded as a symmetry group of strong interaction. To consider combinations of the meson-baryon couplings, it is extremely useful to choose the SU(3)-invariant interaction Lagrangian. Using the matrix representations for the baryon octet, $B$, and meson nonet (singlet state, $M_1$, and octet state, $M_8$), the interaction Lagrangian can be written as a sum of three

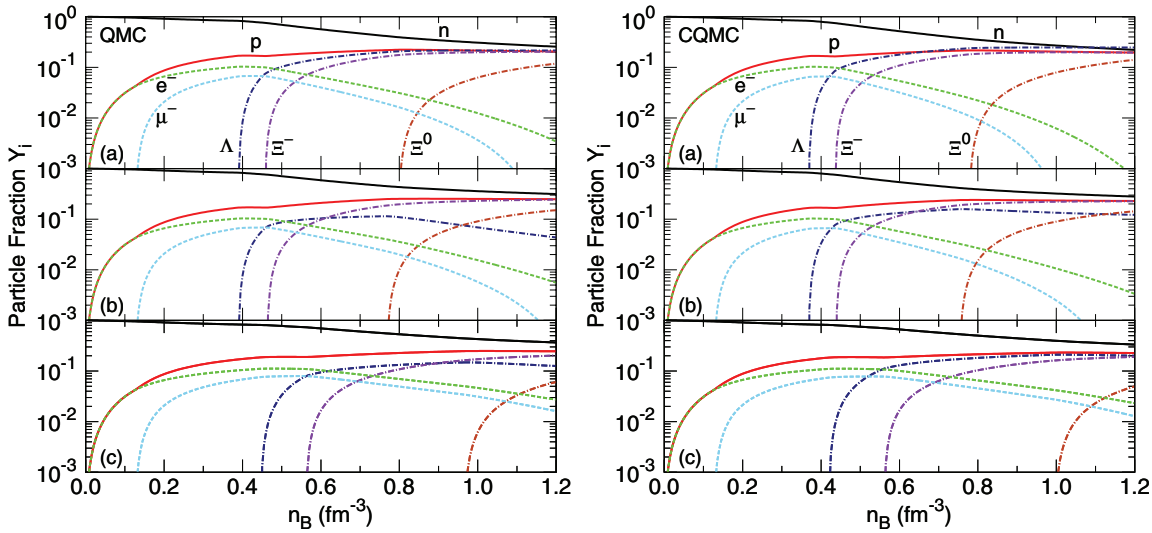


FIG. 1. (Color online) Particle fractions, $Y_i$, in the QMC and CQMC models (left panel, QMC; right panel, CQMC). As explained in the text, in each panel, figure (a) is for the case where only the nonstrange mesons ($\sigma$, $\omega$, and $\rho$) are considered in SU(6) symmetry; figure (b) is for the case where all the mesons, including the $\sigma^*$ and $\phi$, are considered in SU(6) symmetry; and figure (c) is for the case where all the mesons are included in SU(3) symmetry.

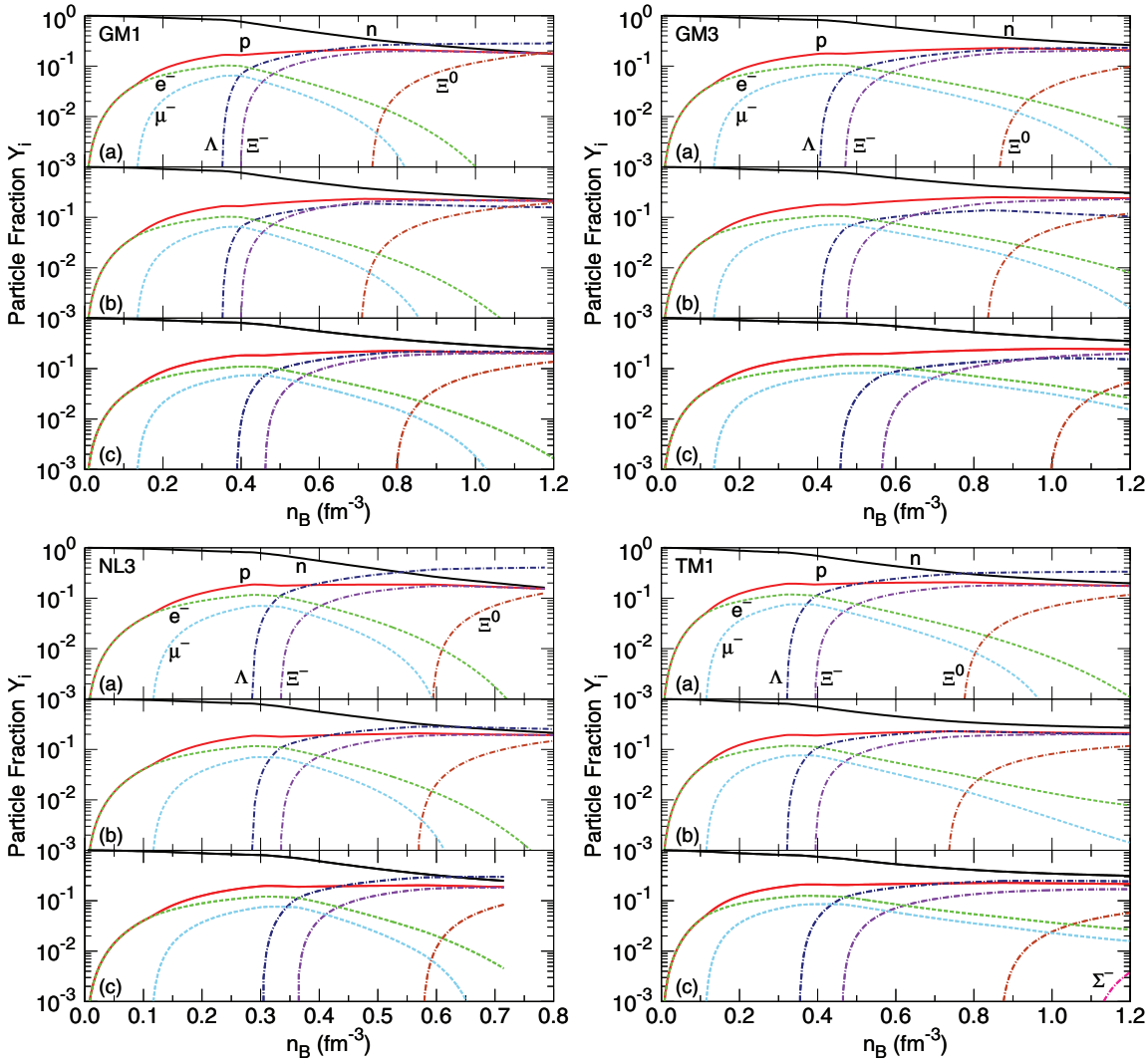


FIG. 2. (Color online) Particle fractions, $Y_i$, in the GM1, GM3, NL3, and TM1 models (upper left panel, GM1; upper right panel, GM3; lower left panel, NL3; lower right panel, TM1). The labels (a), (b), and (c) in the figures are the same as described in the legend of Fig. 1.

terms, namely one coming from the coupling of the meson singlet to the baryon octet ($S$ term) and the other two terms from the interaction of the meson octet and the baryons—one being the antisymmetric ($F$) term and the other being the symmetric ($D$) term [12,30,31]:

$$\mathcal{L}_{\rm int} = -g_8\sqrt{2}[\alpha {\rm Tr}([\bar{B}, M_8]B) + (1-\alpha){\rm Tr}(\{\bar{B}, M_8\}B)] - g_1\frac{1}{\sqrt{3}}{\rm Tr}(\bar{B}B){\rm Tr}(M_1), \quad (21)$$

where $g_1$ and $g_8$ are, respectively, the coupling constants for the meson singlet and octet states, and $\alpha$ ($0 \leqslant \alpha \leqslant 1$) is known as the $F/(F+D)$ ratio. For details, see Refs. [30,31].

We here focus on the isoscalar, vector-meson ($\omega$ and $\phi$) couplings to the octet baryons, because, as usual, the other coupling constants can be determined so as to reproduce the observed properties of nuclear matter and hypernuclei (as discussed in Sec. IV).[1] The physical $\omega$ and $\phi$ mesons are described in terms of the pure singlet, $|1\rangle$, and octet, $|8\rangle$, states as

$$\begin{aligned} \omega &= \cos\theta_v\,|1\rangle + \sin\theta_v\,|8\rangle\,, \\ \phi &= -\sin\theta_v\,|1\rangle + \cos\theta_v\,|8\rangle\,, \end{aligned} \quad (22)$$

with $\theta_v$ being the mixing angle.

In SU(3) symmetry, all possible combinations of the couplings are then determined by four parameters: the singlet and octet coupling constants, $g_1$ and $g_8$, the $F/(F+D)$ ratio for the vector mesons, $\alpha_v$, and the mixing angle, $\theta_v$. If we require the *universality* assumption for the (electric) $F/(F+D)$ ratio, we find $\alpha_v = 1$ [30,32]. In the limit of the

[1]When SU(3) symmetry is applied to the *isovector*, vector mesons, the Fock term is, in fact, necessary to reproduce the observed symmetry energy [11].

*ideal* mixing, the mixing angle is given by

$$\theta_v^{\rm ideal} = \tan^{-1}\left(\frac{1}{\sqrt{2}}\right) \simeq 35.26^\circ. \tag{23}$$

Furthermore, if the coupling ratio, $z$, is chosen to be

$$z \equiv \frac{g_8}{g_1} = \frac{1}{\sqrt{6}} \simeq 0.4082, \tag{24}$$

we can obtain the usual SU(6) relations:

$$\frac{1}{3}g_{\omega N} = \frac{1}{2}g_{\omega\Lambda} = \frac{1}{2}g_{\omega\Sigma} = g_{\omega\Xi}, \tag{25}$$

$$2g_{\phi\Lambda} = 2g_{\phi\Sigma} = g_{\phi\Xi} = \frac{2\sqrt{2}}{3}g_{\omega N}, \quad g_{\phi N} = 0. \tag{26}$$

In the present calculation, we refer to the Nijmegen extended-soft-core (ESC) model [30] to fix the mixing angle and $z$. At present, this model may be the most complete model for the baryon-baryon interaction. It can well describe not only the $N$-$N$ but also the $Y$-$N$ and $Y$-$Y$ interactions in terms of the meson exchanges based on SU(3) symmetry. This model has then suggested the values of $\theta_v$ and $z$ as

$$\theta_v = 37.50^\circ, \quad z = 0.1949. \tag{27}$$

We notice that the mixing angle is very close to the ideal value, while the value of $z$ is much smaller than that in SU(6) symmetry. It may be expected that a small value of $z$ helps enhance the coupling constants [12]. We can find the relations of the coupling constants in SU(3) symmetry as

$$g_{\omega\Lambda} = g_{\omega\Sigma} = \frac{1}{1+\sqrt{3}z\tan\theta_v}g_{\omega N}, \tag{28}$$

$$g_{\omega\Xi} = \frac{1-\sqrt{3}z\tan\theta_v}{1+\sqrt{3}z\tan\theta_v}g_{\omega N},$$

$$g_{\phi N} = \frac{\sqrt{3}z-\tan\theta_v}{1+\sqrt{3}z\tan\theta_v}g_{\omega N}, \tag{29}$$

$$g_{\phi\Lambda} = g_{\phi\Sigma} = \frac{-\tan\theta_v}{1+\sqrt{3}z\tan\theta_v}g_{\omega N},$$

$$g_{\phi\Xi} = -\frac{\sqrt{3}z+\tan\theta_v}{1+\sqrt{3}z\tan\theta_v}g_{\omega N}. \tag{30}$$

Therefore, once the value of $g_{\omega N}$ is given, the other coupling constants, $g_{\omega Y}$ and $g_{\phi B}$, are determined by Eqs. (28)–(30).

## IV. MODELS

We examine two types of RMF models. One is based on the QMC and CQMC models [10,11,23], in which the variation of baryon structure in matter is taken into account. In these models, it is not necessary to consider any NL potential for describing the properties of nuclear matter around the saturation density, $n_B^0$. The other is the QHD-type models with the NL potential given in Eq. (7). In fact, we adopt the parametrizations of the GM1, GM3 [8], NL3 [33], TM1 [34], FSUGold [35], and IU-FSU [36] models. Some of those models are very popular, because they are accurately calibrated by using various experimental data on infinite nuclear matter and finite nuclei.

### A. SU(6) symmetry

In the case of QHD-type, the coupling constants, $g_{\sigma N}$, $g_{\omega N}$, and $g_{\rho N}$, are determined so as to reproduce the binding energy per nucleon, $w_0$, and symmetry energy, $a_4$, at $n_B^0$. The parameters, $g_2$, $g_3$, $c_3$, and $\Lambda_{\omega\rho}$, in Eq. (7) are chosen to be the values given in the original papers. For the vector-meson couplings to hyperons, we use the SU(6) relations given in Eqs. (25) and (26), and the following coupling relations:

$$g_{\rho N} = \tfrac{1}{2}g_{\rho\Sigma} = g_{\rho\Xi}, \quad g_{\rho\Lambda} = 0. \tag{31}$$

Furthermore, assuming that the $\sigma^*$ meson does not couple to a nucleon ($g_{\sigma^* N} = 0$), the couplings of $\sigma$-$Y$ and $\sigma^*$-$Y$ may be determined as follows. In RMF approximation, the potential

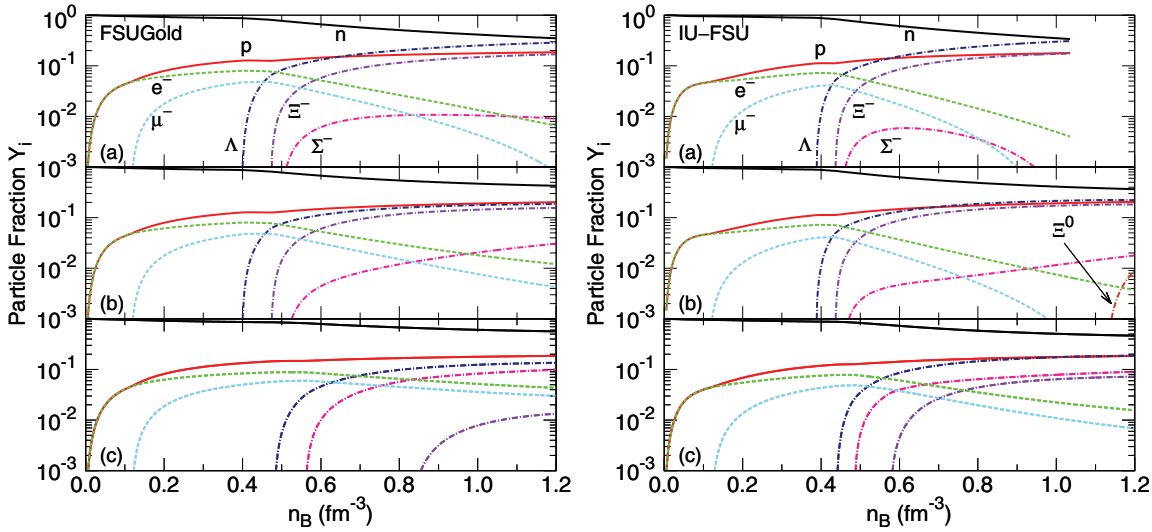


FIG. 3. (Color online) Particle fractions, $Y_i$, in the FSUGold and IU-FSU models (left panel, FSUGold; right panel, IU-FSU). The labels (a), (b), and (c) are the same as described in the legend of Fig. 1.

for hyperon $Y$ in symmetric nuclear matter, $U_Y^{(N)}$, may be calculated as

$$U_Y^{(N)} = -g_{\sigma Y}\bar{\sigma} + g_{\omega Y}\bar{\omega}. \tag{32}$$

Thus, we can determine the coupling constants, $g_{\sigma Y}$, if we take the following values suggested from the experimental data of hypernuclei: $U_\Lambda^{(N)} = -28$ MeV, $U_\Sigma^{(N)} = +30$ MeV, and $U_\Xi^{(N)} = -18$ MeV [37–39].

In addition, if we consider the Nagara event [40], which may suggest that the depth of the potential between two $\Lambda$s is about $-5$ MeV, we may be able to fix the coupling constant, $g_{\sigma^*\Lambda}$, by assuming that $U_\Lambda^{(\Lambda)} \simeq -5$ MeV, where $U_\Lambda^{(\Lambda)}$ is the potential for $\Lambda$ in $\Lambda$-hyperon matter:

$$U_\Lambda^{(\Lambda)} = -g_{\sigma\Lambda}\bar{\sigma}^{(\Lambda)} - g_{\sigma^*\Lambda}\bar{\sigma}^{*(\Lambda)} + g_{\omega\Lambda}\bar{\omega}^{(\Lambda)} + g_{\phi\Lambda}\bar{\phi}^{(\Lambda)}. \tag{33}$$

Here, the superscript $(Y)$ stands for a quantity in $Y$-hyperon matter. Furthermore, we assume the relation, $g_{\sigma^*\Sigma} = g_{\sigma^*\Lambda}$, which is presented by SU(6) symmetry, and determine the coupling constant, $g_{\sigma^*\Xi}$, using the relation $U_\Xi^{(\Xi)} \simeq 2U_\Lambda^{(\Lambda)}$ [38,39].

In the QMC and CQMC models, the NL interaction is not necessary and the coupling constants can be determined by the same way as in the QHD-type model. We, however, notice that in Eqs. (32) and (33), the coupling constants for the scalar mesons should be replaced by the field-dependent ones [see Eqs. (5) and (6)].

In Tables II, III, and IV, we list the coupling constants in SU(6) symmetry and the properties of symmetric nuclear matter at $n_B^0$.

### B. SU(3) symmetry

As discussed in Sec. III, because the pure singlet and octet states are mixed in SU(3) symmetry, the $\phi$ meson, as well as the $\sigma$ and $\omega$ mesons, contributes to the nuclear saturation properties. Thus, we have to readjust the coupling constants to satisfy the saturation condition, namely the binding energy per nucleon, $w_0$, at $n_B^0$. We suppose that $g_{\sigma^*N} = 0$ and the coupling constant, $g_{\sigma N}$, takes the same value as in SU(6) symmetry. The coupling constant, $g_{\rho N}$, is fixed so as to reproduce the value of symmetry energy given in the original paper.

First, we consider the QHD-type models. Assuming that the couplings, $g_2$ and $g_3$, in the NL potential takes the values given in the original paper, we can determine not only $g_{\omega N}$ and $c_3$ but also $g_{\phi N}$ so as to reproduce the same saturation condition as in the original paper. We here notice that, because $g_{\phi N}$ is related to $g_{\omega N}$ through Eq. (29), $g_{\phi N}$ is not free. Even in the case where the quartic term of the $\omega$ field is not involved, namely $c_3 = 0$, it is possible to reproduce the same saturation condition, because the $\phi$-meson contributions to the energy density and pressure are quadratic [see Eqs. (17) and (20)], and they have the same forms as in the $\omega$-meson contributions. For the vector-meson couplings to hyperons, we use the SU(3) relations given in Eqs. (28) and (30), and the relations for the $\rho$ meson, Eq. (31). For the couplings of $\sigma$-$Y$ and $\sigma^*$-$Y$, we may be able to use the same procedure as in SU(6) symmetry.

Next, in the QMC and CQMC models, we can also reproduce the same properties of nuclear matter as in SU(6) symmetry by only readjusting the coupling constant, $g_{\omega N}$ [thus, $g_{\phi N}$ is also varied through Eq. (29)]. The other coupling constants may be determined by the same ways as in SU(6) symmetry.

The results in SU(3) symmetry are also given in Tables II, III, and IV.

## V. NUMERICAL RESULTS AND DISCUSSIONS

### A. Properties of symmetric nuclear matter

As seen in Tables II, III, and IV, the properties of symmetric nuclear matter are well reproduced in all the models.

For the QHD-type models, the results calculated by GM1, GM3, and NL3 are presented in Table III, and those by TM1,

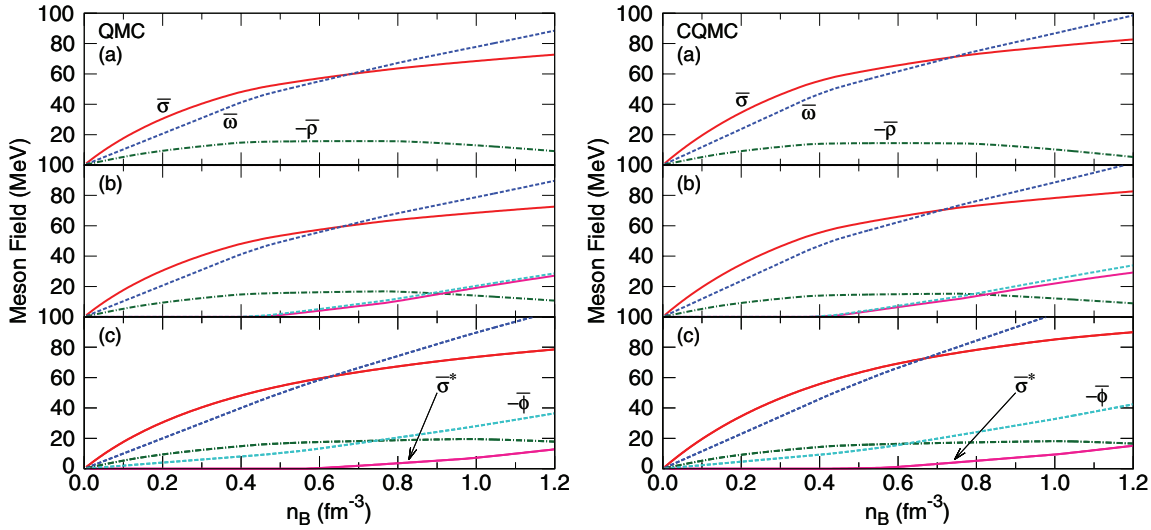


FIG. 4. (Color online) Meson fields in the QMC and CQMC models (left panel, QMC; right panel, CQMC). The labels (a), (b), and (c) are the same as described in the legend of Fig. 1.

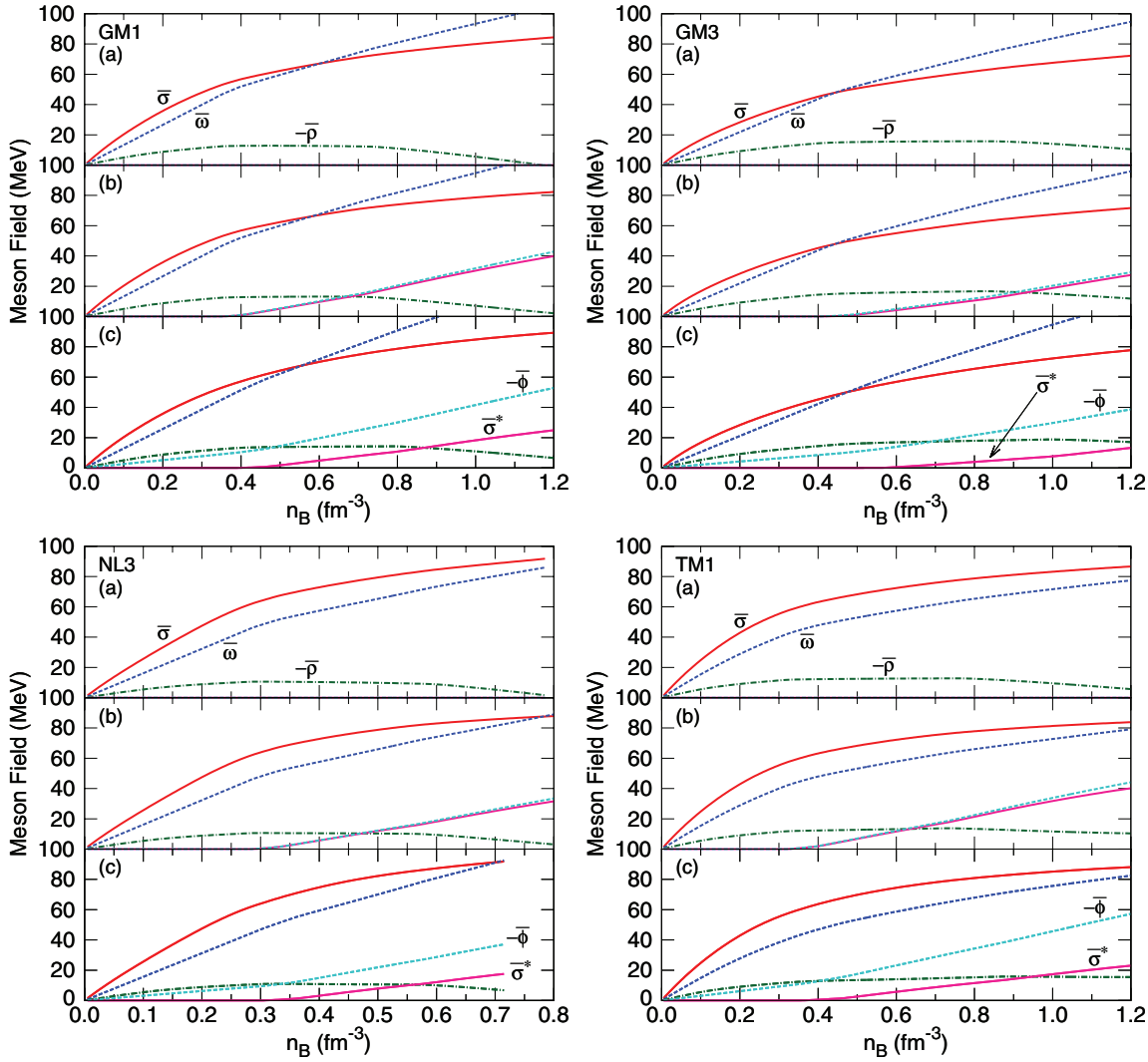


FIG. 5. (Color online) Meson fields in the GM1, GM3, NL3, and TM1 models (upper left panel, GM1; upper right panel, GM3; lower left panel, NL3; lower right panel, TM1). The labels (a), (b), and (c) are the same as described in the legend of Fig. 1.

FSUGold, and IU-FSU are in Table IV. In the former group, the NL potential involves the self-interaction terms of the $\sigma$ meson, while, in the latter group, in addition, the NL terms of the vector ($\omega$ and $\vec{\rho}$) mesons are taken into account. In the GM1, GM3, and NL3 models, the same saturation properties can be achieved in both SU(6) and SU(3) cases, as explained in Sec. IV B [see also Eqs. (10) and (11)]. In contrast, in the TM1, FSUGold, and IU-FSU models, the symmetry energy, incompressibility, and slope parameter, $L$, in SU(3) symmetry are slightly changed from the original values [given in SU(6) symmetry], because the terms of $c_3$ and/or $\Lambda_{\omega\rho}$ in the NL potential, which has the quartic dependence of the nuclear density in the energy density and pressure of matter, also take part in reproducing the saturation condition.

Furthermore, we notice the following two points. Firstly, in the extension of SU(6) to SU(3) symmetry, the coupling, $g_{\omega N}$, becomes smaller, because the (total) repulsive force is attributed not only to the $\omega$ but also to the $\phi$, which is caused by the mixing in Eq. (22). We note that the coupling constant, $g_{\phi N}$, is negative, because the mean-field value of the $\phi$ meson has a negative sign (see Figs. 4–6).

Second, the coupling, $g_{\sigma^* Y}$ (or the $\sigma^*$ field itself), in SU(3) symmetry is suppressed in all the models, compared with that in the SU(6) case. In contrast, the $\sigma$-$Y$ couplings in SU(3) symmetry are more enhanced than in SU(6) symmetry. This enhancement may counterbalance the additional, repulsive force due to the $\phi$ meson in the $Y$-$N$ interaction, because the (total) repulsive force in the SU(3) case is stronger than in the SU(6) case.

### B. Neutron stars

In the core of a neutron star, the charge neutrality and $\beta$ equilibrium under weak processes are imposed in solving the TOV equation [25,26]. To obtain the realistic relation between the mass and radius of a neutron star, for the EoS at very low nuclear densities ($\leqslant 0.068$ fm$^{-3}$), we use the models given by Baym, Bethe, Pethick, and Sutherland [43,44]. In fact, the radius is relatively sensitive to the EoS at low density.

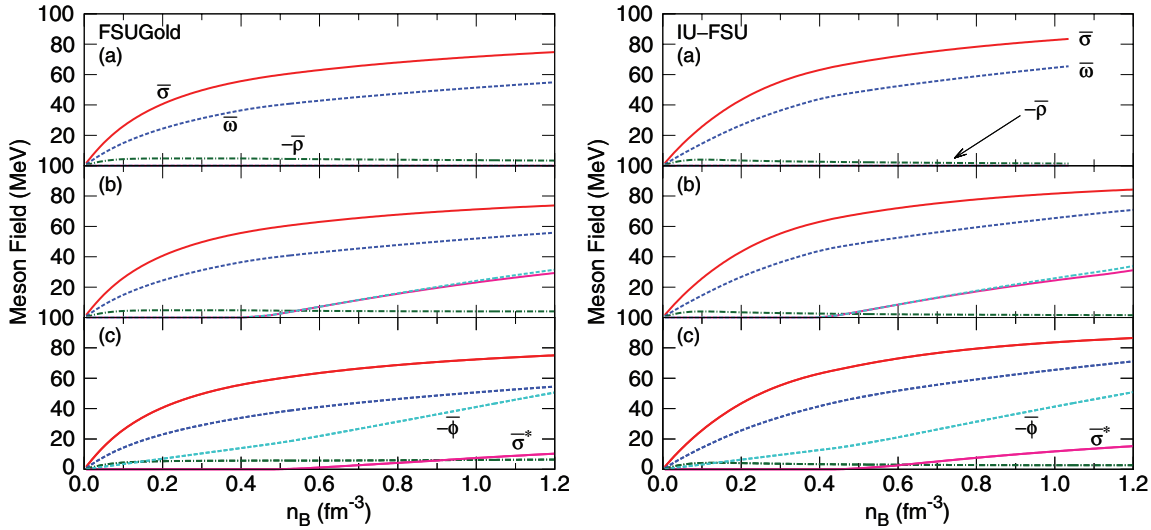


FIG. 6. (Color online) Meson fields in the FSUGold and IU-FSU models (left panel, FSUGold; right panel, IU-FSU). The labels (a), (b), and (c) are the same as described in the legend of Fig. 1.

In the following calculations, we study three cases in each model: (a) only the nonstrange mesons ($\sigma$, $\omega$ and $\rho$) are included in SU(6) symmetry; (b) all the mesons including the $\sigma^*$ and $\phi$ are considered in SU(6) symmetry; (c) all the mesons are included in SU(3) symmetry.

In Figs. 1–3, we show the particle fractions in the core of a neutron star. As seen in the figures, from case (a) to (c), in order, the hyperons are created at higher densities. For example, the threshold densities of the $\Lambda$ and $\Xi^-$ productions in SU(3) symmetry are higher than those in SU(6) symmetry, which makes the fractions of hyperons small at high densities and, thus, increases the neutron fraction.

In the models, except for FSUGold and IU-FSU, the $\Lambda$ and $\Xi^{0,-}$ hyperons are created, but the $\Sigma$ does not appear, because the $\Sigma$-hyperon potential in nuclear matter, $U_\Sigma^{(N)}$, is chosen to be repulsive (see Sec. IV A).[2] However, in the FSUGold and IU-FSU models, because the rather strong $\omega$-$\rho$ (NL) repulsive interaction, $\Lambda_{\omega\rho}\bar{\omega}^2\bar{\rho}^2$, is included [see Eq. (7)], the $\Xi^{0,-}$ fields are very suppressed at high densities (especially, in the SU(3) case), and the $\Sigma^-$ alternatively appears beyond $n_B \simeq 0.4$–$0.6$ fm$^{-3}$. Furthermore, the order of the threshold densities for the $\Xi^-$ and $\Sigma^-$ is reversed in the SU(6) and SU(3) cases. This is a very remarkable phenomenon, and the isoscalar-isovector NL interaction, $\Lambda_{\omega\rho}\bar{\omega}^2\bar{\rho}^2$, plays a unique role in the particle fractions.

We here note that, in some figures, the calculation stops at a certain density because the effective nucleon mass becomes zero beyond that density.

The meson fields are presented in Figs. 4–6. As it should be, in SU(6) symmetry, the strange-meson fields appear in the density region where the hyperons are generated. On the other hand, in SU(3) symmetry, the $\phi$ meson contributes to the baryon interactions even at low densities because of the mixing effect. However, the $\sigma^*$ meson emerges above the density at which the first hyperon (usually the $\Lambda$) is created. This is because we assume that $g_{\sigma^*N} = 0$. In the FSUGold and IU-FSU models, the fields of $\omega$ and $\rho$ mesons (especially the $\rho$) are very suppressed because of the isoscalar-isovector, NL interaction.

In Figs. 7–9, we show the EoS in each model. Furthermore, in Figs. 10–12, we present the mass-radius relation of a neutron star calculated by the TOV equation. The detail of the neutron-star properties is also shown in Table V.

As expected, because the isoscalar, vector-meson couplings to the octet baryons are enhanced in SU(3) symmetry, the extension from SU(6) to SU(3) symmetry hardens the EoS very much. In each model, the hardest EoS is given by case (c), while the softest one is obtained in case (a). This tendency can be related to the fact that, as seen in Figs. 1–3, the densities at which the hyperons appear in case (c) are rather higher than those in case (a). In general, the strange mesons, especially

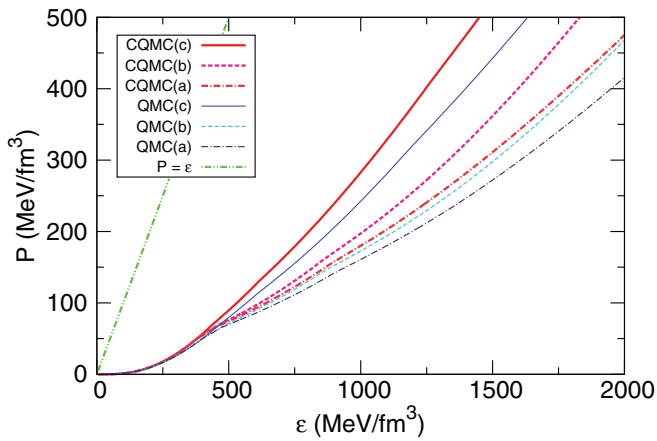


FIG. 7. (Color online) Equations of state in the QMC and CQMC models. The labels (a), (b), and (c) are the same as described in the legend of Fig. 1.

[2]We note that if the Fock term is included [10,11,45], the hyperons except the $\Xi^-$ disappear.

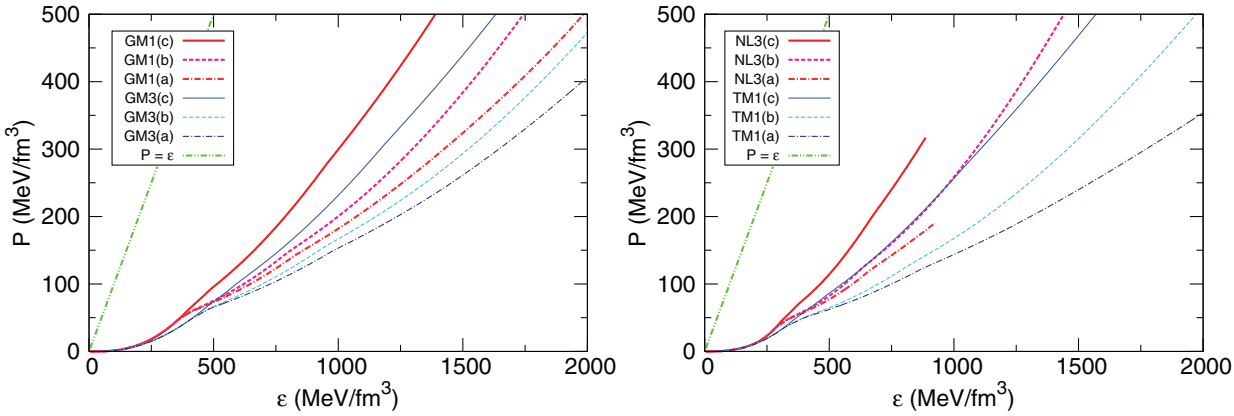


FIG. 8. (Color online) Equations of state in the GM1, GM3, NL3, and TM1 models (left panel, GM1 and GM3; right panel, NL3 and TM1). The labels (a), (b), and (c) are the same as described in the legend of Fig. 1.

the $\phi$ meson, also play an important role in supporting a heavy neutron star. In the mass-radius relations presented in Figs. 10–12, we can again see that, in each model, the maximum neutron-star mass in case (c) is heaviest, while the lightest one is given in case (a). We note that, in Fig. 11, the curve (red solid) for the NL3 model in SU(3) symmetry cannot reach the maximum point because the nucleon mass becomes negative before the maximum point.

We summarize the following several comments on the mass-radius relations shown in Figs. 10–12. In the QMC and CQMC models, the maximum neutron-star masses calculated in SU(3) symmetry are consistent with the pulsars J1614-2230 and/or J0348+0432. In particular, the mass in the CQMC model clearly exceeds the mass of J0348+0432. Because the difference between the QMC and CQMC models is originated by the hyperfine interaction between two quarks inside a baryon, the large difference between the two maximum masses is mainly generated by this microscopic interaction. It is noticeable that the quark-quark hyperfine interaction is very vital to obtain the correct mass spectra of octet baryons in a nuclear medium [15,22].

In the GM1 model, the maximum neutron-star mass in SU(3) symmetry is much larger than the observed masses of J1614-2230 and J0348+0432. In contrast, the maximum mass in the GM3 model is clearly under the observed value (see the left panel in Fig. 11). The difference between the two models is in the values of the nuclear incompressibility and the slope parameter, namely $K_v = 300\,(240)$ MeV and $L = 93.9\,(89.7)$ MeV for the GM1(3) model (see Table III).

The NL3 model is a unique model, in which the mass of J1614-2230 can be explained even in SU(6) symmetry (see the right panel in Fig. 11). This model may be characterized by the large values of symmetry energy ($a_4 = 37.4$ MeV) and slope parameter ($L = 118$ MeV) (see Table III).

The rather large values of $a_4$ and $L$ are also used in the TM1 model, where only the SU(3) result can, however, reach the masses of J1614-2230 and J0348 + 0432. Furthermore, the difference between the maximum masses in SU(6) and SU(3) symmetries is very large in the TM1 model (see also Table V). This fact may be caused by the repulsive force due to the NL $c_3\bar{\omega}^4$ term in Eq. (7). Note that, to reproduce the same saturation condition as in SU(6) symmetry, the strength of $c_3$ in SU(3) symmetry is larger than that in SU(6) symmetry (see Table IV).

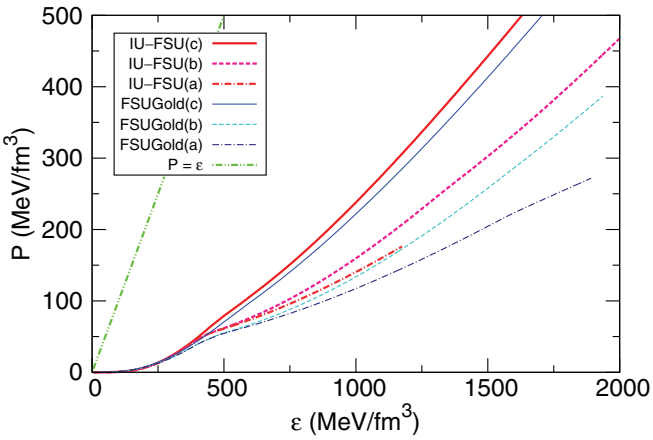


FIG. 9. (Color online) Equations of state in the FSUGold and IU-FSU models. The labels (a), (b), and (c) are the same as described in the legend of Fig. 1.

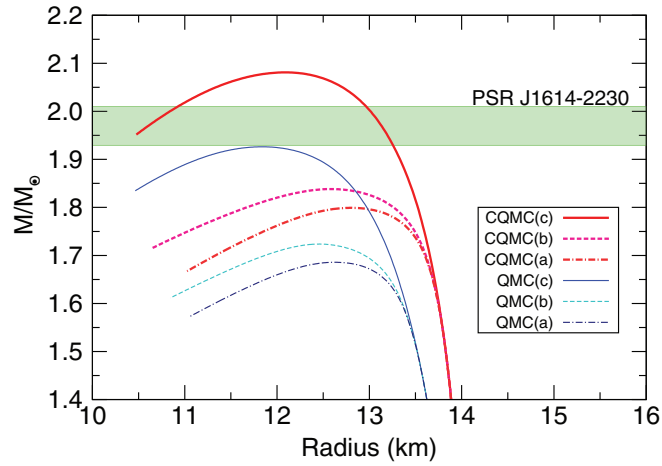


FIG. 10. (Color online) Mass-radius relations in the QMC and CQMC models. The labels (a), (b), and (c) are the same as described in the legend of Fig. 1.

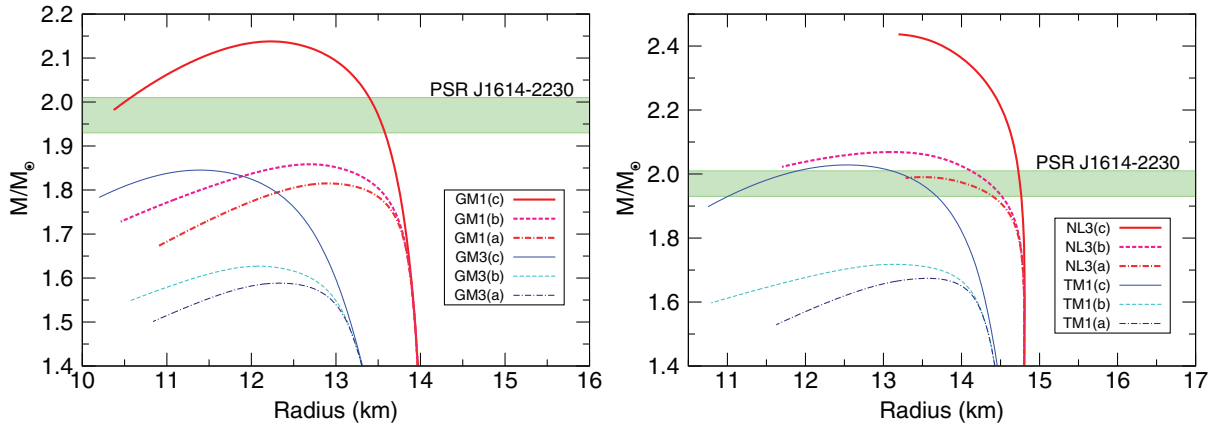


FIG. 11. (Color online) Mass-radius relations in the GM1, GM3, NL3, and TM1 models (left panel, GM1 and GM3; right panel, NL3 and TM1). The labels (a), (b), and (c) are the same as described in the legend of Fig. 1. In the NL3 model, the (red) solid curve for SU(3) symmetry does not yet reach the maximum point because the nucleon mass in matter becomes negative at the endpoint.

Unfortunately, the mass of J1614-2230 cannot be explained by the FSUGold and IU-FSU models. However, in both models the maximum mass in SU(3) symmetry becomes 1.8–1.9 $M_\odot$, which is not far from the observed mass. In these models, the maximum mass in SU(6) symmetry is again very different from the value in SU(3) symmetry (see Table V). Furthermore, although the curves for $M/M_\odot$ in the SU(6) and SU(3) cases normally coincide with each other in the low mass region (see Figs. 10 and 11), the two curves clearly stay away from each other even at $M/M_\odot = 0.8$ in the FSUGold and IU-FSU models (see Fig. 12). These facts may again be caused by the very large difference between the values of $c_3$ in SU(6) and SU(3) symmetries (see Table IV).

Last, we shall see how the uncertainty of the hyperon potentials in nuclear matter (see Sec. IV A) changes the present main results. The potential depth for $\Lambda$ ($U_\Lambda^{(N)} = -28$ MeV) may be more reliable than those for $\Sigma$ and $\Xi$, because the experimental data on $\Lambda$ hypernuclei are rather rich. Therefore, we fix the former, while we shall change the values of the latter potentials by 25%, namely $U_\Sigma^{(N)} = +30 \pm 7.5$ MeV and $U_\Xi^{(N)} = -18 \pm 4.5$ MeV, by readjusting the couplings, $g_{\sigma\Sigma}$ and $g_{\sigma\Xi}$, respectively. In Table VI, we show the variation of neutron-star properties in the FSUGold model. As we can see in Table VI, although the threshold densities at which the hyperons appear show some change (thus, the particle fractions vary a little), the maximum mass and the radius are not much altered. Therefore, the neutron-star mass and radius are not sensitive to the variation of the hyperon potentials, which may be consistent with the findings in Ref. [12].

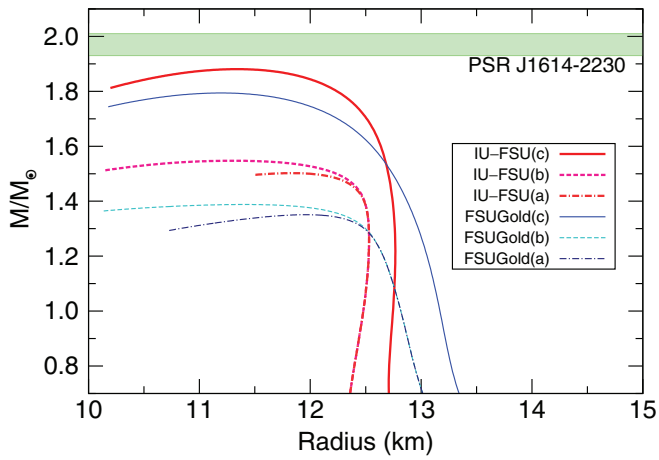


FIG. 12. (Color online) Mass-radius relations in the FSUGold and IU-FSU models. The labels (a), (b), and (c) are the same as described in the legend of Fig. 1.

## VI. SUMMARY

We have calculated the particle fractions, the meson fields, and the EoS in the core of a neutron star, using the popular RMF models (such as GM1, GM3, NL3, TM1, FSUGold, and IU-FSU) as well as the QMC and CQMC models. It is noticeable that some of the RMF models are accurately parametrized to compute the properties of infinite nuclear matter and finite nuclei. On the other hand, because, in the QMC and CQMC models, the quark degrees of freedom in a baryon are taken into account, they allow us to consider the variation of the

TABLE V. Properties of a neutron star in SU(6) or SU(3) symmetry. We list the neutron-star radius, $R_{\max}$ (in km), the ratio of the neutron-star mass to the solar mass, $M_{\max}/M_\odot$, and the central density, $n_c$ (in fm$^{-3}$), at the maximum-mass point. In these calculations, we consider all the mesons ($\sigma$, $\omega$, $\rho$, $\sigma^*$, and $\phi$).

| | SU(6) | | | SU(3) | | |
|---|---|---|---|---|---|---|
| | $R_{\max}$ | $M_{\max}/M_\odot$ | $n_c$ | $R_{\max}$ | $M_{\max}/M_\odot$ | $n_c$ |
| QMC | 12.5 | 1.72 | 0.85 | 11.8 | 1.93 | 0.96 |
| CQMC | 12.6 | 1.84 | 0.84 | 12.1 | 2.08 | 0.90 |
| GM1 | 12.7 | 1.86 | 0.82 | 12.2 | 2.14 | 0.87 |
| GM3 | 12.1 | 1.63 | 0.93 | 11.4 | 1.85 | 1.05 |
| NL3[a] | 13.1 | 2.07 | 0.78 | – | – | – |
| TM1 | 13.1 | 1.72 | 0.77 | 12.5 | 2.03 | 0.86 |
| FSUGold | 11.4 | 1.39 | 1.03 | 11.2 | 1.79 | 1.08 |
| IU-FSU | 11.3 | 1.55 | 1.03 | 11.3 | 1.88 | 1.02 |

[a]In the NL3 model with SU(3) symmetry, the nucleon mass becomes negative before the neutron-star mass reaches the maximum point. Therefore, the maximum mass is not given in SU(3) symmetry.

TABLE VI. Change in the neutron-star properties due to ambiguity of the hyperon potentials. The calculation has been performed in the FSUGold model with SU(3) symmetry. We list the coupling constants, $g_{\sigma\Sigma}$ and $g_{\sigma\Xi}$, for various potential depths, the neutron-star radius, $R_{\max}$ (in km), the ratio of the neutron-star mass to the solar mass, $M_{\max}/M_{\odot}$, and the central density, $n_c$ (in fm$^{-3}$), at the maximum-mass point. Furthermore, we also present the threshold densities, $n^{\rm th}_{\Sigma^-}$ and $n^{\rm th}_{\Xi^-}$ (in fm$^{-3}$), at which the $\Sigma^-$ and $\Xi^-$ are, respectively, created.

| $(U_\Sigma^{(N)}, U_\Xi^{(N)})$ | $g_{\sigma\Sigma}$ | $g_{\sigma\Xi}$ | $n^{\rm th}_{\Sigma^-}$ | $n^{\rm th}_{\Xi^-}$ | $R_{\max}$ | $M_{\max}/M_{\odot}$ | $n_c$ |
|---|---|---|---|---|---|---|---|
| (+22.5, −13.5) | 6.832 | 6.823 | 0.520 | 1.120 | 11.17 | 1.787 | 1.085 |
| (+22.5, −18.0) | 6.832 | 6.953 | 0.520 | 0.955 | 11.17 | 1.787 | 1.085 |
| (+22.5, −22.5) | 6.832 | 7.084 | 0.520 | 0.835 | 11.17 | 1.787 | 1.085 |
| (+30.0, −13.5) | 6.615 | 6.823 | 0.560 | 0.940 | 11.19 | 1.794 | 1.080 |
| (+30.0, −18.0) | 6.615 | 6.953 | 0.560 | 0.825 | 11.20 | 1.794 | 1.075 |
| (+30.0, −22.5) | 6.615 | 7.084 | 0.560 | 0.735 | 11.20 | 1.794 | 1.075 |
| (+37.5, −13.5) | 6.397 | 6.823 | 0.605 | 0.825 | 11.20 | 1.800 | 1.075 |
| (+37.5, −18.0) | 6.397 | 6.953 | 0.605 | 0.740 | 11.20 | 1.800 | 1.075 |
| (+37.5, −22.5) | 6.397 | 7.084 | 0.605 | 0.670 | 11.20 | 1.799 | 1.075 |

quark structure of baryon in dense mater. In particular, the CQMC model involves the quark-quark hyperfine interaction, and, thus, it can correctly describe the octet baryon spectra in matter as well as in vacuum [22].

In the present calculations, we have examined the extension from SU(6) spin-flavor symmetry based on the quark model to SU(3) flavor symmetry in determining the isoscalar, vector-meson couplings to the octet baryons. We have also studied how the strange mesons ($\sigma^*$ and $\phi$) contribute to the internal structure of a neutron star.

In SU(3) symmetry, we have found that the models except GM3, FSUGold, and IU-FSU can explain the masses of J1614-2230 and/or J0348 + 0432. In the GM3, FSUGold, and IU-FSU models, although the maximum mass cannot reach $1.97 \pm 0.04 M_{\odot}$, the calculated mass is not far from that value. Therefore, the extension from SU(6) to SU(3) symmetry and the strange vector meson, $\phi$, are very significant in sustaining a heavy neutron star. In addition, the variation of baryon structure in matter also helps prevent the collapse of a neutron star. We have found that, if those effects are taken into account at the RMF level, a massive neutron star could be sustained even when hyperons exist inside the core.

Because of scarce experimental data on hypernuclei, the meson couplings to hyperons have large ambiguities. We have, thus, examined the sensitivity of the present result to the variation of the hyperon-potential depths using the FSUGold model. Then, we have found that the mass and radius of a neutron star are not much altered even if the potential depths are changed by 25%.

In RMF models, the NL potential, $U_{NL}$, is indispensable for reproducing the saturation condition for symmetric nuclear matter and the properties of finite nuclei. In the present calculations, it involves not only the usual, NL $\sigma$ terms but also the $c_3\bar{\omega}^4$ term and the isoscalar-isovector $\Lambda_{\omega\rho}\bar{\omega}^2\bar{\rho}^2$ term. Among them, in particular, the $c_3\bar{\omega}^4$ term hardens the EoS and, thus, enhances a neutron-star mass. Furthermore, the isoscalar-isovector coupling plays a unique role in the particle fractions inside a neutron star. Because the $\sigma$-$\Sigma$ and $\sigma^*$-$\Sigma$ coupling constants are usually determined so as to fit the (repulsive) mean-field potential for the $\Sigma$ in nuclear matter, it becomes difficult to create the $\Sigma$ hyperon in the core of a neutron star. However, in the FSUGold and IU-FSU models, instead of the $\Xi^{0,-}$, the $\Sigma^-$ can emerge with a considerable fraction even at rather low density.

As the power counting [46,47] suggests, there may be many possible NL couplings and many-body forces containing various meson fields, which may contribute to the EoS. It is, thus, interesting to study how such interactions contribute to the properties of a neutron star. We note that, at the MF level, the NL potential may be regarded as many-body interactions among baryons because the meson fields are just auxiliary fields and, thus, they can be replaced with bilinear forms of baryon fields.

In RMF models, the parametrization is usually performed using experimental data measured around $n_B^0$. However, because the region of 0.8–1.1 fm$^{-3}$ ($>6n_B^0$) may be important in the EoS for a neutron star, no one knows if such parametrizations work correctly at such high densities. Therefore, although in this paper we have studied RMF models from various standpoints, it may be difficult to winnow the correct model out at the RMF level. As suggested in the Dirac-Brueckner-Hartree-Fock calculations [48], it may, at least, be imperative to include the density dependence of the parameters to obtain conclusive results on the EoS.

In the present calculations, we have not considered the Fock (exchange) term. In *naive* QHD-I [27], the Fock contribution seems very small in symmetric nuclear matter. However, it plays a very important role even around the normal nuclear matter density as well as at high densities, if the $\rho$ meson is included and the tensor interaction, thus, arises [10,11]. It is remarkable that, when the tensor interaction is taken into account, the $\Lambda$ hyperon does not appear in the core even at high density [10,11,45]. Furthermore, the tensor contribution is very important in reproducing the density dependence of symmetry energy, $a_4$.

We here note that the strange mesons, $K$ and $K^*$, are not considered in the present calculation, because they do *not* contribute to the EoS, etc., at the relativistic Hartree level. However, if the Fock term is included, they can contribute and mix some baryons in matter. The pion also mixes the $\Sigma$ and $\Lambda$ through the Fock term.

At very high density, the quark and gluon degrees of freedom, rather than the hadron degrees of freedom, may take place in the core matter [49]. Because the degrees of freedom in quark-gluon matter are generally large, it is necessary to assume a rather strong correlation between quarks and gluons to support a massive neutron-star mass. It would be very interesting to investigate how the quark-gluon phase connects with the hadron one and how such degrees of freedom contribute to the EoS for a neutron star.

## ACKNOWLEDGMENT

This work was supported by the National Research Foundation of Korea (Grants No. 2012M7A1A2055605 and No. 2011-0015467).

[1] W. Baade and F. Zwicky, Phys. Rev. **46**, 76 (1934).
[2] A. Hewish and S. E. Okoye, Nature (London) **207**, 59 (1965).
[3] J. M. Lattimer and M. Prakash, Phys. Rep. **442**, 109 (2007).
[4] J. H. Taylor and J. M. Weisberg, Astrophys. J. **345**, 434 (1989).
[5] J. M. Weisberg, D. J. Nice, and J. H. Taylor, Astrophys. J. **722**, 1030 (2010).
[6] P. Demorest, T. Pennucci, S. Ransom, M. Roberts, and J. Hessels, Nature (London) **467**, 1081 (2010).
[7] J. Antoniadis *et al.*, Science **340**, 448 (2013).
[8] N. K. Glendenning and S. A. Moszkowski, Phys. Rev. Lett. **67**, 2414 (1991).
[9] J. Schaffner-Bielich, Nucl. Phys. A **804**, 309 (2008).
[10] T. Miyatsu, T. Katayama, and K. Saito, Phys. Lett. B **709**, 242 (2012).
[11] T. Katayama, T. Miyatsu, and K. Saito, Astrophys. J. Suppl. **203**, 22 (2012).
[12] S. Weissenborn, D. Chatterjee, and J. Schaffner-Bielich, Phys. Rev. C **85**, 065802 (2012); Nucl. Phys. A **881**, 62 (2012).
[13] P. A. M. Guichon, Phys. Lett. B **200**, 235 (1988).
[14] K. Saito and A. W. Thomas, Phys. Lett. B **327**, 9 (1994).
[15] S. Nagai, T. Miyatsu, K. Saito, and K. Tsushima, Phys. Lett. B **666**, 239 (2008).
[16] K. Saito, AIP Conf. Proc. **1261**, 238 (2010).
[17] K. Saito, K. Tsushima, and A. W. Thomas, Phys. Rev. C **55**, 2637 (1997).
[18] P. A. M. Guichon, K. Saito, E. Rodionov, and A. W. Thomas, Nucl. Phys. A **601**, 349 (1996).
[19] W. K. Brooks, S. Strauch, and K. Tsushima, J. Phys. Conf. Ser. **299**, 012011 (2011).
[20] K. Saito, K. Tsushima, and A. W. Thomas, Nucl. Phys. A **609**, 339 (1996).
[21] K. Tsushima, K. Saito, J. Haidenbauer, and A. W. Thomas, Nucl. Phys. A **630**, 691 (1998).
[22] T. Miyatsu and K. Saito, Prog. Theor. Phys. **122**, 1035 (2010).
[23] T. Miyatsu and K. Saito, Few-Body Syst., doi: 10.1007/s00601-012-0567-z, arXiv:1209.3360 [nucl-th].
[24] K. Saito, K. Tsushima, and A. W. Thomas, Prog. Part. Nucl. Phys. **58**, 1 (2007).
[25] R. C. Tolman, Proc. Nat. Acad. Sci. USA **20**, 169 (1934); [Gen. Rel. Grav. **29**, 935 (1997)].
[26] J. R. Oppenheimer and G. M. Volkoff, Phys. Rev. **55**, 374 (1939).
[27] B. D. Serot and J. D. Walecka, Adv. Nucl. Phys. **16**, 1 (1986).
[28] G. A. Lalazissis, T. Nikšić, D. Vretenar, and P. Ring, Phys. Rev. C **71**, 024312 (2005).
[29] A. Sulaksono and B. K. Agrawal, Nucl. Phys. A **895**, 44 (2012).
[30] T. A. Rijken, M. M. Nagels, and Y. Yamamoto, Prog. Theor. Phys. Suppl. **185**, 14 (2010).
[31] J. J. de Swart, Rev. Mod. Phys. **35**, 916 (1963); **37**, 326(E) (1965).
[32] T. A. Rijken, V. G. J. Stoks, and Y. Yamamoto, Phys. Rev. C **59**, 21 (1999).
[33] G. A. Lalazissis, J. Konig, and P. Ring, Phys. Rev. C **55**, 540 (1997).
[34] Y. Sugahara and H. Toki, Nucl. Phys. A **579**, 557 (1994).
[35] B. G. Todd-Rutel and J. Piekarewicz, Phys. Rev. Lett. **95**, 122501 (2005).
[36] F. J. Fattoyev, C. J. Horowitz, J. Piekarewicz, and G. Shen, Phys. Rev. C **82**, 055803 (2010).
[37] J. Schaffner and I. N. Mishustin, Phys. Rev. C **53**, 1416 (1996).
[38] J. Schaffner, C. B. Dover, A. Gal, C. Greiner, D. J. Millener, and H. Stoecker, Annals Phys. **235**, 35 (1994).
[39] F. Yang and H. Shen, Phys. Rev. C **77**, 025801 (2008).
[40] H. Takahashi *et al.*, Phys. Rev. Lett. **87**, 212502 (2001).
[41] M. Dutra, O. Lourenço, J. S. Sá Martins, A. Delfino, J. R. Stone, and P. D. Stevenson, Phys. Rev. C **85**, 035201 (2012).
[42] M. B. Tsang *et al.*, Phys. Rev. C **86**, 015803 (2012).
[43] G. Baym, H. A. Bethe, and C. Pethick, Nucl. Phys. A **175**, 225 (1971).
[44] G. Baym, C. Pethick, and P. Sutherland, Astrophys. J. **170**, 299 (1971).
[45] D. L. Whittenbury, J. D. Carroll, A. W. Thomas, K. Tsushima, and J. R. Stone, arXiv:1204.2614 [nucl-th].
[46] H. Mueller and B. D. Serot, Nucl. Phys. A **606**, 508 (1996).
[47] R. J. Furnstahl, B. D. Serot, and Hua-Bin Tang, Nucl. Phys. A **615**, 441 (1997).
[48] E. V. Dalen and H. Müther, Int. J. Mod. Phys. E **19**, 2077 (2010).
[49] N. K. Glendenning, *Compact Stars*, 2nd ed. (Springer-Verlag, New York, 2000).